JOINT EUROPEAN TORUS

JET–P(90)74

JET Team
(presented by P.E. Stott)

Recent Results from JET

Recent Results from JET

The JET Team
(presented by P.E. Stott)

JET-Joint Undertaking, Culham Science Centre, OX14 3DB, Abingdon, UK

** See Appendix 1*

Prcprint of an Invited Paper presented to the 32nd Meeting of the Division of Plasma Physics
of the American Physical Society (Cincinnati, Ohio, USA,, 12-16th November 1990)

RECENT RESULTS FROM JET

The JET Team[1] (presented by P E Stott)
JET Joint Undertaking, Abingdon, Oxon OX14 3EA, UK.

ABSTRACT

The latest results obtained in the JET experiment are summarized. Discharges with the fusion triple product $n_D(0)\tau_E T_i(0) \approx 9.5 \pm 0.5\times10^{20}m^{-3}skeV$ have been achieved. In deuterium plasmas the reaction rate is $R_{DD} \approx 7.3\times10^{16}s^{-1}$ corresponding to $Q_{DD} \approx 2.4\times10^{-3}$. Simulations of the fusion yield in mixed deuterium and tritium plasmas predict $0.85 < Q_{DT} < 0.95$. This is close to the point of break-even and within a factor 6 of the value required for ignition. These results have been obtained by careful optimization of the tokamak operating conditions and by exploiting various new machine facilities to further improve plasma purity and to enhance the efficiency of ion cyclotron heating. The results of detailed experiments to improve understanding of tokamak physics are also reported.

INTRODUCTION

Good progress continues to be made in pursuit of JET's objective to obtain and study plasmas in conditions and with dimensions approaching those needed in a fusion reactor. Discharges have been achieved with $R_{DD} \approx 7.3\times10^{16}s^{-1}$ and with the fusion triple product $n_D(0)\tau_E T_i(0) \approx 9.5 \pm 0.5\times10^{20}m^{-3}skeV$ (within a factor of 6 of the value required for a DT fusion reactor). Figure 1 shows the interior of the torus during preparations for the 1990 experimental campaign. The ion cyclotron heating antennas, beryllium belt limiters, carbon inner wall tiles and sections of beryllium tiles at the lower X-point can be seen.

During 1990 the experimental program has concentrated on three areas; (i) the introduction and exploitation of new facilities, (ii) improving the understanding of tokamak physics, (iii) improving plasma performance. The main new facilities are beryllium screens on the ion cyclotron resonance heating (ICRH) antennas, beryllium tiles at the lower X-point, feedback control of the plasma position with respect to the ICRH antennas, lower hybrid current drive and helium neutral beam injection. Experiments aimed at improving the understanding of tokamak physics have covered a wide range of topics including detailed studies of thermal, particle and impurity transport, and various

aspects of H-mode physics. Experiments to improve performance have concentrated on high current limiter and inner wall discharges, and on optimizing the the fusion performance of X-point discharges.

NEW MACHINE FACILITIES

Plasma Purity

During the first few years of JET's operation, extensive areas of the inconel torus walls, including the belt limiters, inner wall and X-point interaction regions, were covered with carbon tiles. Other surfaces were carbonized. Beryllium was introduced in 1989, first as a thin layer evaporated onto the carbon surfaces from four sources equally spaced around the torus mid-plane, and later with solid beryllium tiles on the belt limiters. Oxygen and carbon impurity concentrations in the plasma were strongly reduced, leading to lower Z_{eff} and higher n_D/n_e. Density control was previously a problem in JET with all-carbon surfaces, but beryllium was found to pump both hydrogen and helium, giving better density control and the possibility of using strong gas puffing to maintain a low edge temperature with reduced beryllium influx.

Nickel Faraday screens on the ICRH antennas were previously the source of a serious influx of impurity during ICRH which prevented the plasma entering the H-mode with ICRH alone. H-modes heated by ICRH were obtained in 1989 when these nickel surfaces were covered with a thin evaporated beryllium film. For the 1990 experimental programme, the nickel screens have been replaced by beryllium screens. The operational range of H-modes with ICRH in both dipole and monopole antenna configurations has been extended. Further improvement to ICRH in the X-point configuration is obtained by a new position feedback system that maintains a constant plasma coupling impedance. This is effective in allowing high power ICRH (up to 10MW) to be maintained through the transition from L to H mode. H-modes heated by ICRH have confinement properties comparable to those with neutral beam heating.

Beryllium X-point Tiles

The lower X-point protection tiles have been changed from carbon to beryllium, although the shape of the beryllium tiles, which had been machined already for a different purpose, was not optimized for the power flux at the X-point. H-mode discharges have been obtained with similar power thresholds and comparable confinement properties to discharges on the upper set of carbon

tiles. As with carbon, H-modes on the beryllium tiles are terminated by "blooms" due to the formation of localized "hot-spots" on the tiles. Various techniques to delay the onset of the blooms have been explored, including sweeping the X-point radially in order to distribute the power over a larger tile area. Carbon blooms are effectively suppressed in conditions of high recycling at the upper divertor tiles. The high recycling regime can be established by gas puffing either before or during the H-mode, but it is found to be more stable when the gas puffing is started before the high power neutral beam heating. The high recycling regime is improved when the X-point is well inside the vacuum vessel, but otherwise there appears to be no clear systematic dependence of the H-mode duration on the position of the X-point.

A quantitative comparison between H-modes with carbon and beryllium tiles is inconclusive at the present time because the beryllium tiles became badly melted during the first series of experiments (as already noted, the shape of these beryllium tiles was not optimized for the X-point power flux) and subsequently it was not possible to establish an H-mode on the damaged tiles. These experiments will be continued during 1991 using new carbon and beryllium tiles specifically designed for the X-point region.

Lower Hybrid Current Drive

A lower hybrid current drive (LHCD) system capable of launching 10MW at 3.7MHz is being prepared for JET. Initial experiments have coupled up to 1.6MW to the plasma for up to 20s. A significant drop in the loop voltage corresponding to a non inductive current of about 1MA was achieved at plasma densities up to $3\times10^{19}m^{-3}$. Adding LHCD to a 2MA discharge with 4MW ICRH extended the monster sawtooth period from 0.5s (without LHCD) to 2.9s (with LHCD).

High Current Discharges

Plasma currents of 7MA were achieved in 1988[2] using simultaneous ramps of toroidal field and plasma current to maintain $q_\psi \approx 2.5$. The variation of toroidal field prevented heating during the current rise. A faster current ramp at constant $q_\psi \approx 3.5$ has been developed and extended to 7MA discharges. These discharges have longer flat tops (3s compared to 2s for the earlier 7MA discharges) and adequate flux remains in the core to extend the flat top further in future experiments. Valuable experience of operating tokamaks at high currents near to stability limits has been gained.

Helium Neutral Beam Injection

Helium neutral beam injection with argon frost pumping of the beam line has been demonstrated. Up to 5MW of ^{3}He and 7MW of ^{4}He at 120keV have been injected into 5MA limiter and 3.5MA double null plasmas for up to 3s. Although a low level of localized heating is observed on the lower belt limiter, there are no indications of serious problems such as increased impurities or limiter heating due to the ionization of metastable neutrals in the beam. Helium injection is interesting because beam penetration at these energies (presently 120keV, though future plans include increasing the beam energy to 160keV) is excellent over the typical range of JET plasma densities. Preliminary results show that stored plasma energy and global energy confinement with He beams are comparable to those with D beams. There are several motivations for He injection[3]. The elimination of beam-beam and beam-plasma reactions results in a significant reduction in the neutron yield. This is advantageous in reducing vessel activation and in permitting a more direct interpretation of neutron diagnostic measurements of thermal neutrons. The He injection also provides a precise particle source for alpha particle transport studies and for ion cyclotron minority heating.

IMPROVED UNDERSTANDING

Sawteeth

Sawteeth determine the central plasma parameters and thus the fusion performance. Neutron emission profiles show a dramatic change following a sawtooth collapse (figure 2). In discharges where the neutron emission is mainly thermal, there is a correspondingly large change in the total neutron yield consistent with the loss of thermal ions from the core. In discharges where there are significant non-thermal contributions from beam-plasma and beam-beam reactions, the neutron emission profile also shows a dramatic change, though there is a much smaller drop (typically $< 20\%$) in the total neutron yield. Careful examination of the neutron profiles reveals that after the collapse, the fast ions appear to be redistributed but not completely expelled from the core.

Sawteeth have been suppressed in JET discharges for up to 5s following pellet injection, both during the current rise phase and during the flat top[4]. Polarimetric measurements indicate that the current profile is broadened by the change in electron temperature due to the pellet ablation so that $q_0 > 1$. Long sawtooth-free periods up to 5s have also been obtained in discharges

where q_0 is significantly less than unity ($0.6 < q_0 < 0.8 \pm 0.15$). These "monster sawteeth" are produced most efficiently when the ICRH is applied at the magnetic axis. Sawteeth are not stabilized when the heating is moved outside $q \simeq 1$. The stabilization mechanism is not fully understood but there is strong evidence that fast ions play an a important role. Sawtooth stabilization is an important factor in optimizing the fusion performance as will be discussed later.

Particle and Energy Transport

Electron cyclotron emission and microwave reflectometry have been used to make simultaneous localized measurements of electron temperature and density perturbations propagating in the plasma following sawteeth crashes and due to modulation of the ICRH power during sawteeth free ("monster sawteeth") periods. The data have been analyzed in terms of a linearized electron transport matrix. The diagonal terms correspond to the incremental particle and heat diffusivities, D_e^{inc} and χ_e^{inc}. The off-diagonal terms are a measure of the coupling between heat and particle transport and indicate that pure temperature perturbations are not eigenmodes. Thus if a pure temperature perturbation is launched, it will generate a density perturbation that will be transported at the same rate as the temperature perturbation even though D_e^{inc} and χ_e^{inc} have different values.

Impurity Transport

The transport of various elements including Si, Ar, Xe, Kr, He and several high Z elements, has been studied using gas injection and laser ablation. Impurities injected into the private flux region of X-point plasmas are retained in the divertor. High Z impurities injected at the mid plane penetrate and accumulate in the core, although there is some retention in the divertor when He and Ar are injected at the mid plane. An interesting discovery during these experiments is that inert gases are strongly pumped by beryllium surfaces. In particular, helium is pumped as strongly as deuterium. The pumping mechanism is not fully understood, but it probably involves co-deposition of beryllium.

Alpha Particle Transport

Helium beam injection has been used as an axial particle source to simulate alpha particle diffusion in L- and H-modes. The time and space resolved profiles of helium densities showing the evolution of the injected helium and

the subsequent recycling are measured with charge exchange spectroscopy. In L-mode discharges, the central helium density decays promptly after the He source is switched-off. In H-mode discharges the He concentration decreases more slowly and in some cases is seen to accumulate in the plasma core.

IMPROVEMENT OF FUSION PERFORMANCE

Limiter Discharges

It has been reported previously that the energy confinement in high current, low q limiter discharges in JET is close to L-mode. Enhancement of the fusion yield requires strongly peaked temperature and density profiles. Sawtooth stabilization using ICRH during the current rise of 5MA discharges has now been extended well into the flat top by using a faster current ramp at constant $q_\psi \approx 3.5$ and exploiting the density control provided by beryllium. Strongly peaked electron temperature profiles with $T_e(0) \approx 12$keV are obtained, though with modest ion temperature $T_i(0) \approx 5$keV. A comparison of 3 and 5MA sawtooth-free discharges with similar input power and density shows a steeper temperature gradient, indicating a lower value of χ_e, in the 5MA discharge.

Gas fueled discharges with beryllium limiters have flat density profiles even with beam refueling. Refueling with deeply penetrating pellets is required to produce peaked density profiles. Careful timing of the pellets and heating is needed in order to obtain good penetration. Central electron densities $n_e(0) \approx 2.3\times10^{20}m^{-3}$ have been obtained by injecting a string of 4mm diameter pellets into a 5MA discharge. When heating (6MW of ICRH and 2MW of NBI) is applied, the central density decays fairly rapidly to $n_e(0) \approx 6\times10^{19}m^{-3}$ with $T_e(0) \approx T_i(0) \approx 5$keV and a transient peak $Q_{DD} \approx 5\times10^{-4}$. It is interesting to note that the global energy confinement time is enhanced transiently by ≈30% compared to a gas fueled discharge. Higher ion temperatures with $T_i(0) \approx 18$keV have been obtained with beam heating and pellet refueling in 3MA limiter plasmas. The profiles are strongly peaked; ($T_i(0)/\langle T_i\rangle \approx 7$ and $n_e(0)/\langle n_e\rangle \approx 4$) and the fusion yield is enhanced by a factor ≈ 3 compared to an L-mode discharge with flat profiles, even though the global confinement is not enhanced significantly.

Further development of higher current limiter discharges has continued with the aim of combining peaked profiles with the favorable scaling of global confinement time with current. Sawteeth have been suppressed well into the flat top of a 6MA discharge and during the current rise of a 7MA discharge. A central electron temperature $T_e(0) \approx 9$keV was obtained in both cases. The ions

have been heated by neutral beams in a 6.5MA discharge [figure 3], giving $T_i(0) \approx 7.5$keV, $T_e(0) \approx 8.0$keV and $n_e(0) \approx 5\times10^{19}$. The confinement time is 0.65s giving $n_D(0)\tau_E T_i(0) \approx 2.1\times10^{20}m^{-3}$skeV. This phase of high fusion performance is terminated by a sawtooth crash with a subsequent strong density rise and influx of beryllium.

Inner wall Discharges

The inner wall of JET is protected by approximately $12m^2$ of carbon tiles. The plasma shape must be carefully matched to the curvature of the inner wall in order to avoid carbon blooms due to localized overheating of the tiles. In optimized discharge conditions, neutral beam heating powers up to 16.5MW have been applied for up to 2s without a strong carbon influx. Evaporation of beryllium onto the carbon tiles gives significant improvements in plasma purity and density control. Neutral beam injection into low density ($n_e(0) \approx 3.0\times10^{19}m^{-3}$) target plasmas with $I_P = 4.7$MA gives hot-ion ($T_i(0) \approx 20$keV ,$T_e(0) \approx 9$keV), L-mode discharges with $\tau_E \approx 0.45$s, $n_D(0)\tau_E T_i(0) \approx 2.3\times10^{20}m^{-3}$skeV and $Q_{DD} \approx 1.0\times10^{-3}$.

At lower plasma currents ($I_p < 3$MA) and low toroidal fields, H-mode transitions are obtained in inner wall plasmas. The characteristics of the transition are similar to those at the H-mode transition in X-point discharges. The power threshold of inner wall H-modes is approximately twice that of an X-point H-mode and scales linearly with the toroidal field. The inner wall H-mode appears to be ELM free but the maximum duration is 0.8s.

X-point Discharges

Global energy confinement times in JET H-mode discharges are 2 to 3 times longer than in L-mode. An H-mode data base has been compiled recently with data from JET and 5 other machines of different sizes. The preliminary analysis[5] of these data gives an H-mode scaling law

$$\tau_E = 0.082\ I_P^{1.02} B_T^{0.15} P_L^{-0.47} A^{0.5} R^{1.6} K^{-0.19}.$$

The distribution of radiated power at the X-point and the power and particle fluxes to the tile surface depend on the direction of the toroidal field. When the toroidal field direction is such that the ∇B drift of the ions is *towards* the X-point, the temperature rise at the outer strike point is larger than at the inner strike point. When the toroidal field is reversed, so that the ion drift is *away from* the X-point, the tile temperatures at both strike points

are lower and nearly equal. The carbon bloom is delayed significantly. Langmuir probe measurements of the ion saturation currents to the plates show similar asymmetry (typically a factor 3 greater current to the outer strike point compared to the inner strike point) when the ∇B drift is towards the X-point, whereas the currents at each strike point are almost equal when the drift is reversed. The radiated power is greater at the inner strike zone when ∇B is towards the X-point and at the outer strike zone when ∇B is away from the X-point. The power threshold for the H-mode is lower by a factor ≈ 2 when the ∇B drift is towards the X-point (as observed in other tokamaks) and increases more slowly with B_T. In practice this is unimportant when the emphasis is on high power discharges that are well above the power threshold. The confinement properties (figure 4) and impurity behavior appear to be independent of the field direction.

Two routes have been explored to optimize fusion yield in JET H-modes. The first seeks to combine the good global confinement properties of the H-mode with peaked profiles produced by pellet fueling and central heating[6]. A typical discharge is shown in figure 5. A peaked density profile produced by injecting a string of pellets is heated by a mixture of beams (2.5MW) and ICRH (9MW) to produce peaked temperature profiles with $T_e(0) \approx T_i(0) \approx 10 \pm 1$keV which, although transient, persist into the H-mode phase. The fusion reaction rate peaks at $R_{DD} \approx 1.9\times10^{16}s^{-1}$ corresponding to $Q_{DD} \approx 9.8\times10^{-4}$ and is estimated to be about 90% thermal during the period when the peaked profiles and H-mode phases overlap. The enhancement in fusion yield due to peaked profiles is shown in Figure 6.

The second route to high fusion yield is the hot-ion H-mode obtained when powerful neutral beams are injected into a low density target plasma. In the example shown in figure 7, a single null, 3.5MA discharge is heated by 18MW of D^0 (10MW at 80keV and 8MW at 140keV). The central ion temperature $T_i(0) \approx 28$keV and the plasma energy $W \approx 11.3$MJ. These discharges have obtained the best fusion performance with $Q_{DD} = 2.4\times10^{-3}$ and $n_D\tau_E T_i = 9.5\times10^{20}m^{-3}$skeV.

D(^{3}He) Fusion Experiments.

Fusion powers $\approx$ 140kW were measured from the D^{3}He fusion reaction. These experiments used ion cyclotron heating of the ^{3}He minority and best results were obtained with low ^{3}He concentrations admitted by gas puffing. Centrally deposited ^{3}He from beam injection actually decreased the reaction rate, indicating that the optimum minority concentration is low (<1%) so that the fast particle energy is maximized.

Extrapolation to D-T Plasmas

The range of values of Q_{DD} that have been covered by JET during 1990 is shown in figure 8. The marked points indicate the best values that have been obtained in the four different operating regimes that have been described in this paper (hot ion H-modes, H-mode with peaked density and temperature profiles, belt limiter and inner wall limiter discharges). Simulations[7] of Q_{DT} have been made using the $1\frac{1}{2}$d transport code TRANSP with the assumption that the plasma conditions remain the same as presently achieved in deuterium discharges. The results indicate that it will be necessary to inject both D and T beams in order to ensure an optimum mixture of fuel throughout the plasma cross-section. Several simulations with mixed D and T neutral beams injected into a D + T target plasma give $0.85 < Q_{DT} < 0.95$.

CONCLUSIONS

Further enhancements of the fusion performance of JET has been achieved by exploiting new machine facilities and optimizing the tokamak operating conditions in several discharge configurations (Table I). The hot-ion H-mode has the highest fusion performance with $R_{DD} \approx 7.3\times10^{16}s^{-1}$ producing approximately 50kW of fusion power corresponding to $Q_{DD} \approx 2.4\times10^{-3}$. Simulations of mixed deuterium and tritium plasmas predict $0.85 < Q_{DT} < 0.95$. The fusion triple product $n_D(0)\tau_E T_i(0) \approx 9.5 \pm 0.5\times10^{20}m^{-3}skeV$ is within a factor of 6 of the value required for a DT fusion reactor. Actual fusion powers of 140kW have been produced using the D^3He reaction in discharges with ion cyclotron heating.

Neutral beam injection of ^3He and ^4He has been developed as an alternative to deuterium beam injection and offers a useful operational advantage in reducing the neutron induced activation of the vacuum vessel due to high performance discharges. Detailed studies of tokamak physics have included a comparison of alpha particle transport and retention in L and H-mode discharges, measurements of energy and particle transport coefficients and studies of sawtooth stabilization.

ACKNOWLEDGEMENTS

The contributions of D Campbell, J G Cordey, J Jacquinot, P J Lomas, F B Marcus, A Tanga and K Thomsen during the preparation of this paper are gratefully acknowledged. The pellet injection experiments were carried out under a collaborative agreement between JET and the United States Department of Energy.

REFERENCES

[1]Rebut, P-H., and the JET Team, Proc. of 13th Int. Conf on Plasma Phys. and Cont. Nucl. Fus. Res., (Washington, USA, 1990), Paper IAEA-CN-53/A-1-2.

[2]Bickerton R.J. and the JET Team, Plasma Physics and Cont. Nucl. Fusion Research., Proc 12th IAEA Conf, Nice, **1** (1988) 41.

[3]F. B. Marcus et. al., JET Report JET-R(90)01.

[4]Campbell, D.J. and the JET Team, Proc. of 13th Int. Conf. on Plasma Phys. and Contr. Fus. Res., (Washington, USA, 1990), Paper IAEA-CN-53/A-6-3.

[5]Cordey, J.G., et al, Proc. of 13th Int. Conf. on Plasma Phys. and Contr. Nucl Fus. Res., (WAshington, USA, 1990), Paper IAEA-CN-53/?

[6]Tubbing B J D et al JET-P(90)67 (Submitted for publication in Nucl Fusion).

[7]P M Stubberfield et al., JET-P(90)47 (to be published in Plasma Physics & Controlled Fusion)

TABLE I

COMPARISON OF HIGH PERFORMANCE DISCHARGES

	Hot-Ion H-Mode	PEP H-Mode	Inner Wall	Belt Limiter
Configuration	Single Null [VB drift away from X-point]	Double Null	Carbon Inner Wall + Be Gettering	Beryllium Belt Limiter
Shot number	22689	22490	22202	20934
I_p (MA)	3.6	3.0	4.7	3.1
B_T (T)	2.8	2.8	3.0	3.4
P_{TOT} (MW)	18.0	11.3	16.0	27.5
W_{DIA} (MJ)	11.3	8.3	6.0	7.5
$T_e(0)$ (keV)	10.0	10.0	9.0	8.0
$T_i(0)$ (keV)	28 ± 1.0	9.5 ± 1.0	20.0	7.5
$n_D(0)$ (m^{-3})	4.0×10^{19}	8.0×10^{19}	2.5×10^{19}	5.0×10^{19}
τ_E (s)	0.85	1.0	0.45	0.3
$n_D(0)\ \tau_E\ T_i(0)$ (m^{-3} skeV)	$9.5 \pm 0.5 \times 10^{20}$	$7.8 \pm 0.7 \times 10^{20}$	2×10^{20}	1×10^{20}
R_{DD} (s^{-1})	7.3×10^{16}	1.9×10^{16}	2.8×10^{16}	4.1×10^{16}
Q_{DD}	2.4×10^{-3}	9.8×10^{-4} (90% thermal)	1.0×10^{-3}	8.7×10^{-4}

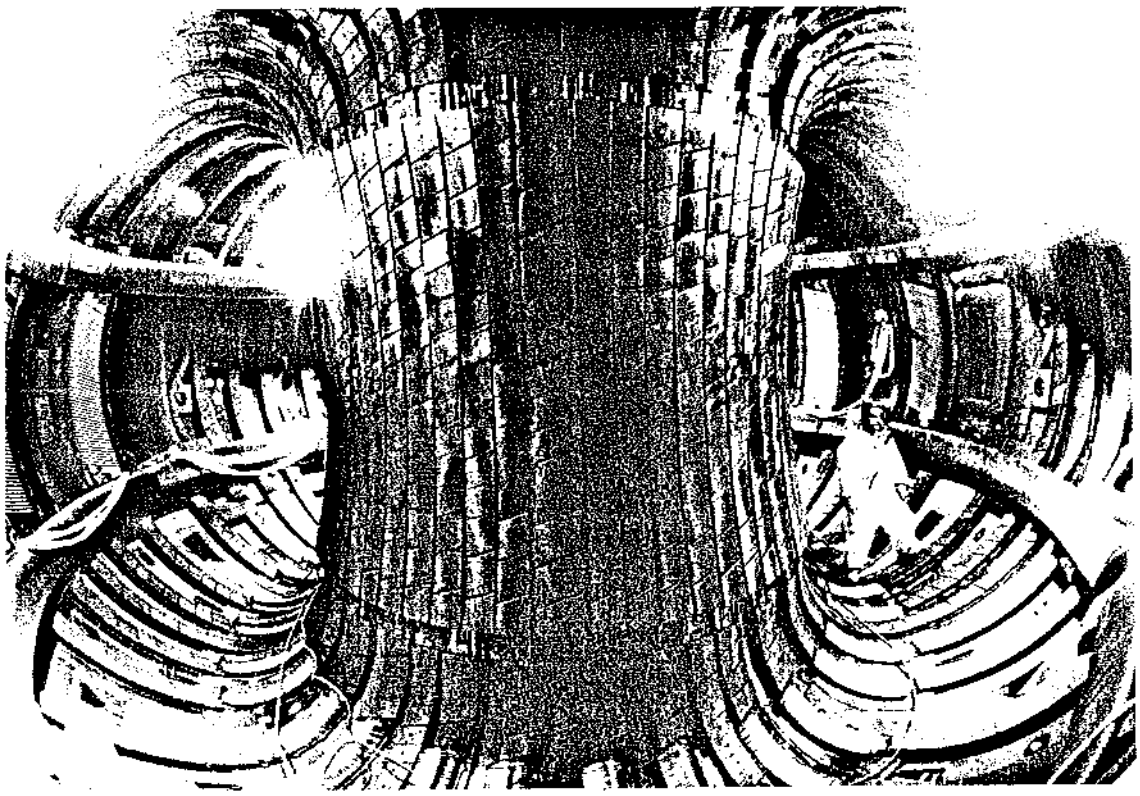

Figure 1 View of the inside of the JET torus in preparation for the 1990 experimental campaign, showing the carbon inner wall tiles, beryllium belt limiters and ICRH antenna screens. Sections of beryllium tiles can be seen at the lower X-point interaction region.

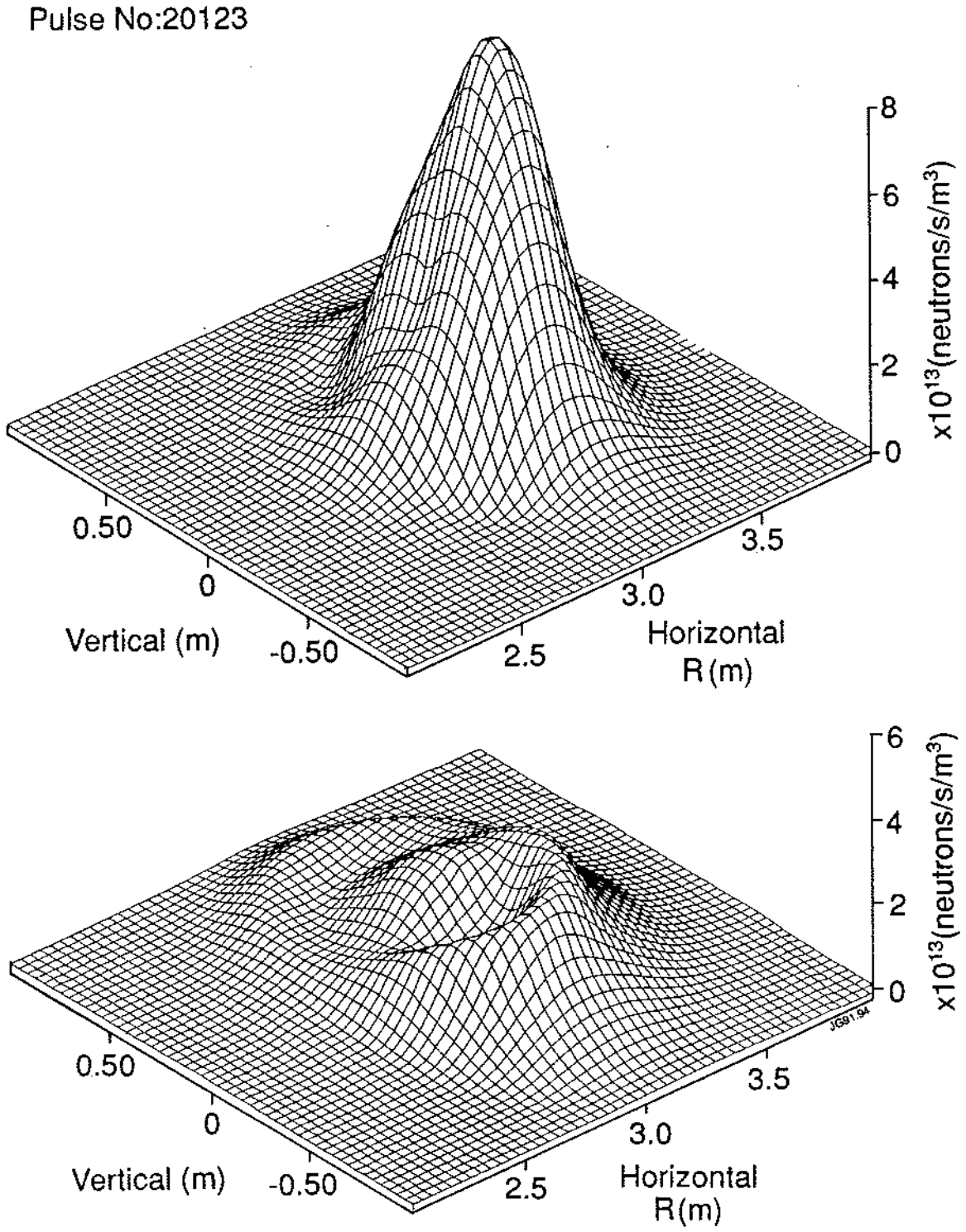

Figure 2 Effect of a sawtooth crash on the neutron yield profile for a 3.1MA discharge with 13.7MW ion cyclotron heating (^{3}He minority). Before the sawtooth crash $T_i(0) \approx 7.0 \pm 0.5$keV and $T_e(0) \approx 5.8$keV.

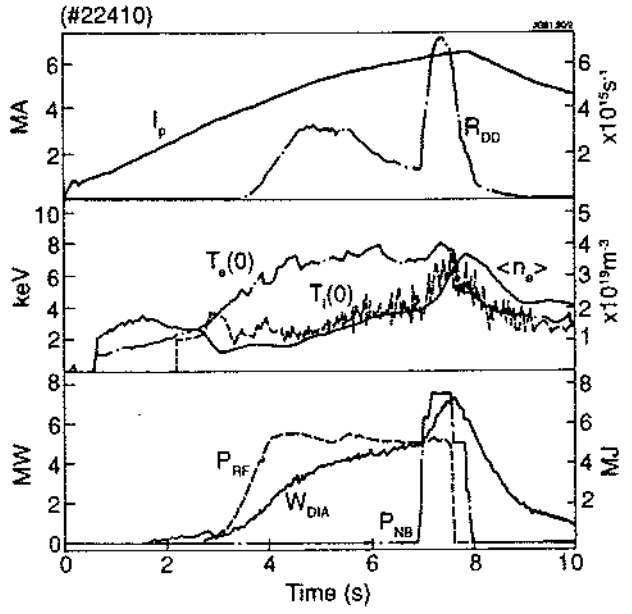

Figure 3 A high current (6.5MA) discharge on the beryllium belt limiters. Combined ion cyclotron and neutral beam heating (total input power ≈ 15MW) gives $T_i(0) \approx 7.5$keV, $T_e(0) \approx 8.0$keV, $n_D(0) \approx 5.0\times10^{19}m^{-3}$, $\tau_E \approx 0.65$s and $n_D(0)\tau_E T_i(0) \approx 2.1\times10^{20}m^{-3}$skeV.

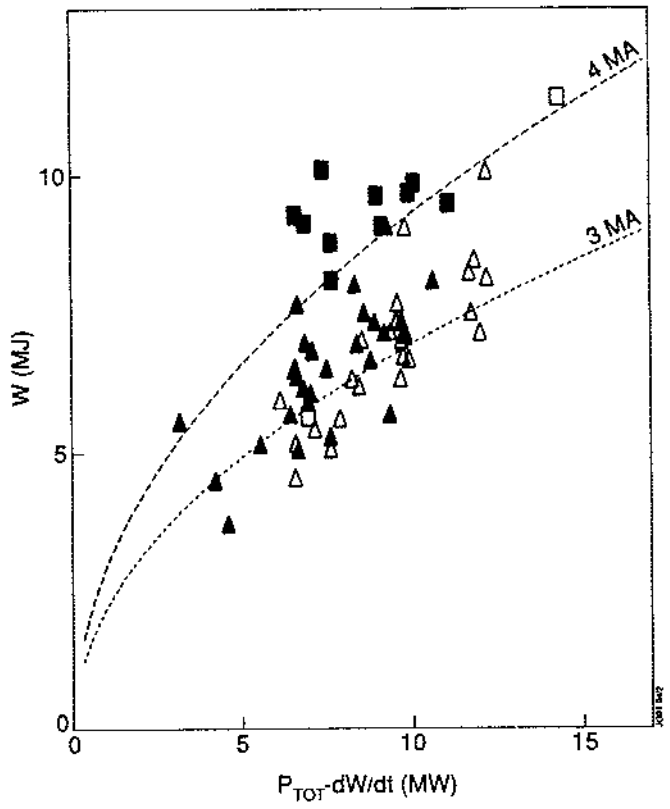

Figure 4 Plasma energy vs power for single null H-modes (triangles I_p = 3MA, squares I_p = 4MA) showing that confinement is similar for discharges with the ∇B ion drift away from the X-point (open points) and towards the X-point (solid points). The lines indicate the ITER H-mode scaling ($\tau_E = 0.082\ I_p^{1.02} B_T^{0.15} P_L^{-0.47} A^{0.5} R^{1.6} K^{-0.19}$) for JET parameters.

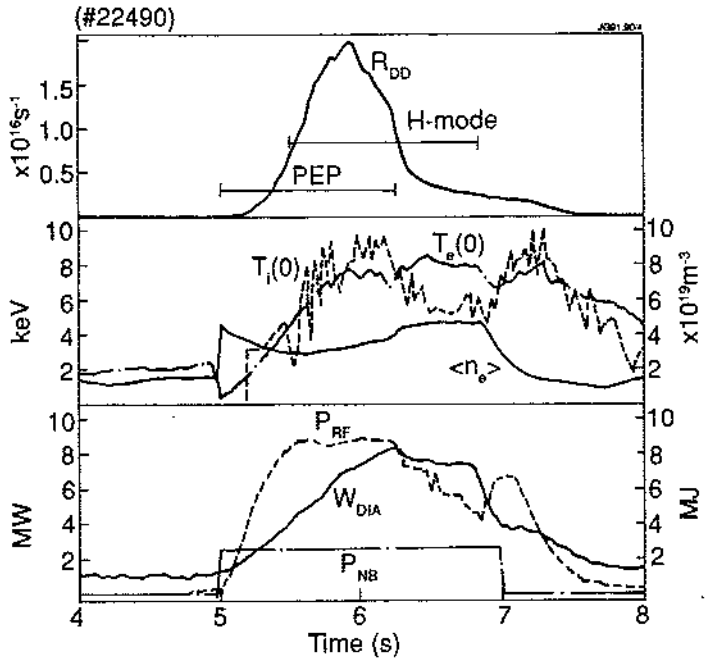

Figure 5 Combination of peaked profiles "PEP mode" produced by pellet injection and central heating by ICRH with the good global energy confinement of the H-mode. The maximum fusion reaction rate ($R_{DD} \approx 1.9 \times 10^{16} s^{-1}$) occurs during the period when the two modes overlap. Other discharge parameters are given in Table I.

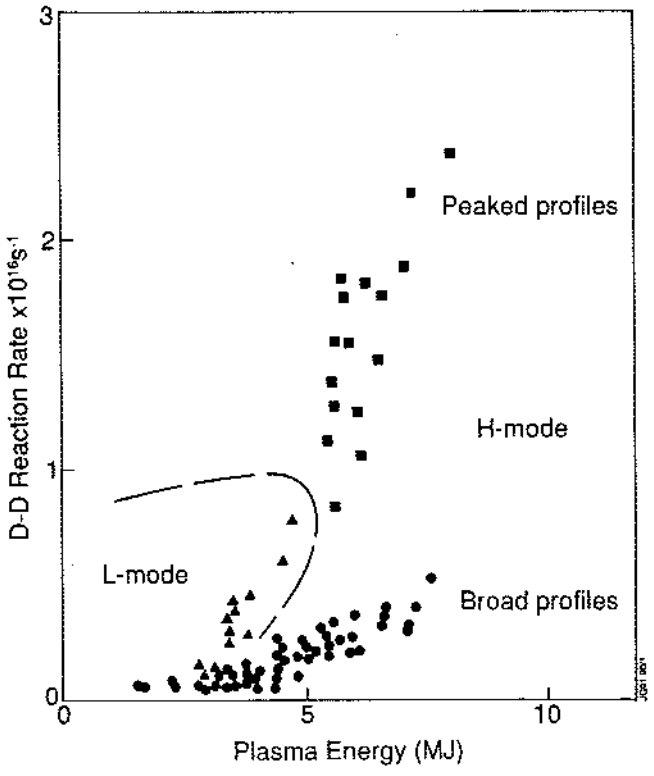

Figure 6 Enhancement of the fusion reaction rate for ICRH H-modes with peaked profiles compared to broad profiles with the same plasma kinetic energy.

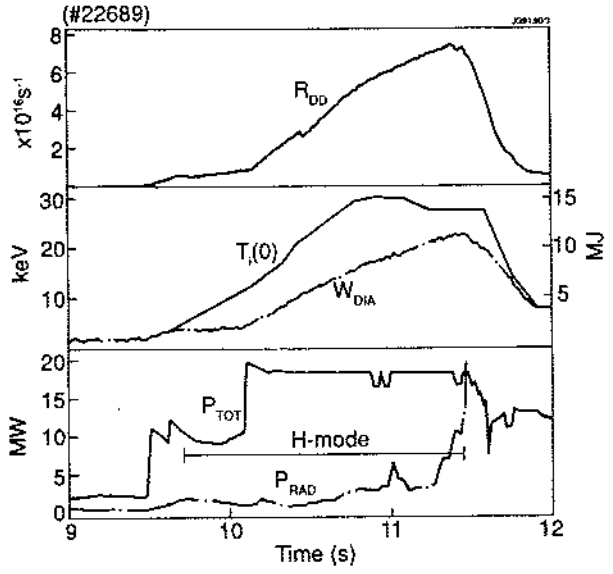

Figure 7 A hot ion ($T_i(0) \approx 28 \pm 1$keV) H-mode ($I_p = 3.5$MA, $B_T = 2.8$T) with 18MW of deuterium neutral beam heating. The maximum stored kinetic energy is $\approx$ 11.3MJ and $n_D(0)\tau_E T_i(0) \approx 9.5 \pm 0.5 \times 10^{20} m^{-3}$skeV. The peak D-D fusion reaction rate is $\approx 7.3 \times 10^{16} s^{-1}$ and $Q_{DD} \approx 2.4 \times 10^{-3}$. Other discharge parameters are given in Table I.

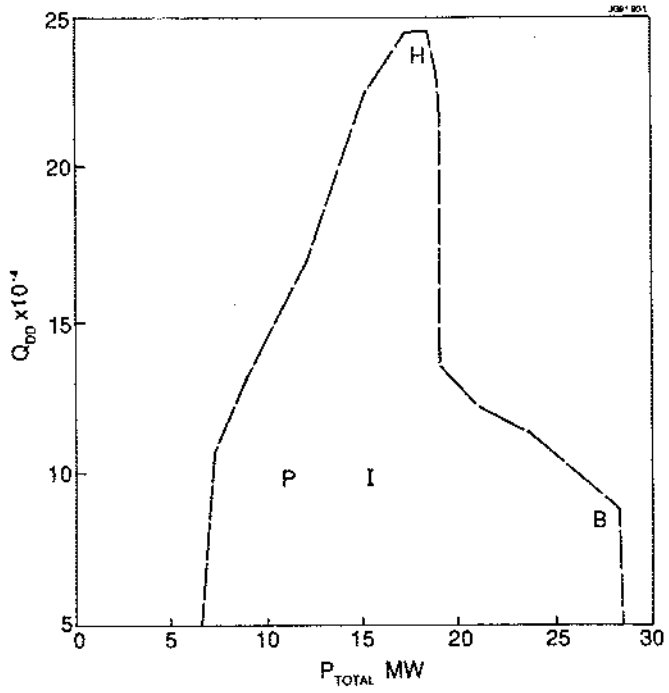

Figure 8 Q_{DD} plotted against the total heating power. The range covered by JET experiments during 1990 is indicated. The marked points indicate four specific discharges (see Table I) that are typical of the different regimes in which high fusion yields have been obtained.

"H" a hot ion, H-mode (figure 7),

"P" H-mode combined with peaked profiles (figure 5),

"I" a hot-ion, L-mode discharge on the inner wall,

"B" a belt limiter discharge with high (28MW) input power.

APPENDIX 1.

THE JET TEAM

JET Joint Undertaking, Abingdon, Oxon, OX14 3EA, U.K.

J.M.Adams[1], F.Alladio[4], H.Altmann, R.J.Anderson, G.Appruzzese, W.Bailey, B.Balet, D.V.Bartlett, L.R.Baylor[24], K.Behringer, A.C.Bell, P.Bertoldi, E.Bertolini, V.Bhatnagar, R.J.Bickerton, A.Boileau[3], T.Bonicelli, S.J.Booth, G.Bosia, M.Botman, D.Boyd[31], H.Brelen, H.Brinkschulte, M.Brusati, T.Budd, M.Bures, T.Businaro[4], H.Buttgereit, D.Cacaut, C.Caldwell-Nichols, D.J.Campbell, P.Card, J.Carwardine, G.Celentano, P.Chabert[27], C.D.Challis, A.Cheetham, J.Christiansen, C.Christodoulopoulos, P.Chuilon, R.Claesen, S.Clement[30], J.P.Coad, P.Colestock[6], S.Conroy[13], M.Cooke, S.Cooper, J.G.Cordey, W.Core, S.Corti, A.E.Costley, G.Cottrell, M.Cox[7], P.Cripwell[13], F.Crisanti[4], D.Cross, H.de Blank[16], J.de Haas[16], L.de Kock, E.Deksnis, G.B.Denne, G.Deschamps, G.Devillars, K.J.Dietz, J.Dobbing, S.E.Dorling, P.G.Doyle, D.F.Düchs, H.Duquenoy, A.Edwards, J.Ehrenberg[14], T.Elevant[12], W.Engelhardt, S.K.Erents[7], L.G.Eriksonn[5], M.Evrard[2], H.Falter, D.Flory, M.Forrest[7], C.Froger, K.Fullard, M.Gadeberg[11], A.Galetsas, R.Galvao[8], A.Gibson, R.D.Gill, A.Gondhalekar, C.Gordon, G.Gorini, C.Gormezano, N.A.Gottardi, C.Gowers, B.J.Green, F.S.Griph, M.Gryzinski[26], R.Haange, G.Hammett[6], W.Han[9], C.J.Hancock, P.J.Harbour, N.C.Hawkes[7], P.Haynes[7], T.Hellsten, J.L.Hemmerich, R.Hemsworth, R.F.Herzog, K.Hirsch[14], J.Hoekzema, W.A.Houlberg[24], J.How, M.Huart, A.Hubbard, T.P.Hughes[32], M.Hugon, M.Huguet, J.Jacquinot, O.N.Jarvis, T.C.Jernigan[24], E.Joffrin, E.M.Jones, L.P.D.F.Jones, T.T.C.Jones, J.Källne, A.Kaye, B.E.Keen, M.Keilhacker, G.J.Kelly, A.Khare[15], S.Knowlton, A.Konstantellos, M.Kovanen[21], P.Kupschus, P.Lallia, J.R.Last, L.Lauro-Taroni, M.Laux[33], K.Lawson[7], E.Lazzaro, M.Lennholm, X.Litaudon, P.Lomas, M.Lorentz-Gottardi[2], C.Lowry, G.Magyar, D.Maisonnier, M.Malacarne, V.Marchese, P.Massmann, L.McCarthy[28], G.McCracken[7], P.Mendonca, P.Meriguet, P.Micozzi[4], S.F.Mills, P.Millward, S.L.Milora[24], A.Moissonnier, P.L.Mondino, D.Moreau[17], P.Morgan, H.Morsi[14], G.Murphy, M.F.Nave, M.Newman, L.Nickesson, P.Nielsen, P.Noll, W.Obert, D.O'Brien, J.O'Rourke, M.G.Pacco-Düchs, M.Pain, S.Papastergiou, D.Pasini[20], M.Paume[27], N.Peacock[7], D.Pearson[13], F.Pegoraro, M.Pick, S.Pitcher[7], J.Plancoulaine, J-P.Poffé, F.Porcelli, R.Prentice, T.Raimondi, J.Ramette[17], J.M.Rax[27], C.Raymond, P-H.Rebut, J.Removille, F.Rimini, D.Robinson[7], A.Rolfe, R.T.Ross, L.Rossi, G.Rupprecht[14], R.Rushton, P.Rutter, H.C.Sack, G.Sadler, N.Salmon[13], H.Salzmann[14], A.Santagiustina, D.Schissel[25], P.H.Schild, M.Schmid, G.Schmidt[6], R.L.Shaw, A.Sibley, R.Simonini, J.Sips[16], P.Smeulders, J.Snipes, S.Sommers, L.Sonnerup, K.Sonnenberg, M.Stamp, P.Stangeby[19], D.Start, C.A.Steed, D.Stork, P.E.Stott, T.E.Stringer, D.Stubberfield, T.Sugie[18], D.Summers, H.Summers[20], J.Taboda-Duarte[22], J.Tagle[30], H.Tamnen, A.Tanga, A.Taroni, C.Tebaldi[23], A.Tesini, P.R.Thomas, E.Thompson, K.Thomsen[11], P.Trevalion, M.Tschudin, B.Tubbing, K.Uchino[29], E.Usselmann, H.van der Beken, M.von Hellermann, T.Wade, C.Walker, B.A.Wallander, M.Walravens, K.Walter, D.Ward, M.L.Watkins, J.Wesson, D.H.Wheeler, J.Wilks, U.Willen[12], D.Wilson, T.Winkel, C.Woodward, M.Wykes, I.D.Young, L.Zannelli, M.Zarnstorff[6], D.Zasche[14], J.W.Zwart.

PERMANENT ADDRESS

1. UKAEA, Harwell, Oxon. UK.
2. EUR-EB Association, LPP-ERM/KMS, B-1040 Brussels, Belgium.
3. Institute National des Récherches Scientifique, Quebec, Canada.
4. ENEA-CENTRO Di Frascati, I-00044 Frascati, Roma, Italy.
5. Chalmers University of Technology, Göteborg, Sweden.
6. Princeton Plasma Physics Laboratory, New Jersey, USA.
7. UKAEA Culham Laboratory, Abingdon, Oxon. UK.
8. Plasma Physics Laboratory, Space Research Institute, Sao José dos Campos, Brazil.
9. Institute of Mathematics, University of Oxford, UK.
10. CRPP/EPFL, 21 Avenue des Bains, CH-1007 Lausanne, Switzerland.
11. Risø National Laboratory, DK-4000 Roskilde, Denmark.
12. Swedish Energy Research Commission, S-10072 Stockholm, Sweden.
13. Imperial College of Science and Technology, University of London, UK.
14. Max Planck Institut für Plasmaphysik, D-8046 Garching bei München, FRG.
15. Institute for Plasma Research, Gandhinagar Bhat Gujat, India.
16. FOM Instituut voor Plasmafysica, 3430 Be Nieuwegein, The Netherlands.
17. Commissiariat à L'Energie Atomique, F-92260 Fontenay-aux-Roses, France.
18. JAERI, Tokai Research Establishment, Tokai-Mura, Naka-Gun, Japan.
19. Institute for Aerospace Studies, University of Toronto, Downsview, Ontario, Canada.
20. University of Strathclyde, Glasgow, G4 ONG, U.K.
21. Nuclear Engineering Laboratory, Lapeenranta University, Finland.
22. JNICT, Lisboa, Portugal.
23. Department of Mathematics, Univeristy of Bologna, Italy.
24. Oak Ridge National Laboratory, Oak Ridge, Tenn., USA.
25. G.A. Technologies, San Diego, California, USA.
26. Institute for Nuclear Studies, Swierk, Poland.
27. Commissiariat à l'Energie Atomique, Cadarache, France.
28. School of Physical Sciences, Flinders University of South Australia, South Australia SO42.
29. Kyushi University, Kasagu Fukuoka, Japan.
30. Centro de Investigaciones Energeticas Medioambientales y Techalogicas, Spain.
31. University of Maryland, College Park, Maryland, USA.
32. University of Essex, Colchester, UK.
33. Akademie de Wissenschaften, Berlin, DDR.

CR 88.49.1A